Influence of Surface Reaction Rate on the Size Dispersion of Interfacial Nanostructures

Rahul V. Magan and Radhakrishna Sureshkumar*

Department of Chemical Engineering and Materials Research Laboratory, Washington University, St. Louis, Missouri 63130

Bin Lin

Department of Chemical Engineering and Materials Science, University of Minnesota, Minneapolis, Minnesota 55455

Received: January 31, 2003; In Final Form: June 3, 2003

Brownian Dynamics (BD) simulations of instantaneous nucleation followed by diffusion-controlled growth of metal nanoparticles on surfaces have shown that a regular distribution of nucleation sites on the surface leads to a reduction in particle size dispersion. However, for several applications, the distribution of active sites on the surface is irregular and random. We use BD simulations to investigate the influence of surface reaction rate on the development of size dispersion of interfacial nanostructures that form by irreversible deposition of noninteracting particles onto surfaces with randomly distributed nucleation sites. The macroscopic balance between the surface reaction rate and bulk diffusion is incorporated into the BD simulations by using a reaction probability that approaches unity in the case of instantaneous, diffusion-limited deposition. It is found that the size uniformity of the growing particles on the randomly distributed active sites can be improved by decreasing the reaction probability. The overlap of diffusion zones surrounding the growing particles, referred to as interparticle diffusional coupling, is responsible for the particle size dispersion in diffusion-controlled growth on randomly distributed sites. The simulation results, in qualitative agreement with experiments, show that reducing the reaction probability is an effective means to reduce the interparticle diffusion coupling, and thereby reduce the particle size dispersion. This could be accomplished by manipulating the process variables that influence the surface reaction rate and/or the bulk diffusivity of the particles.

1. Introduction

The control of the morphology of growing nanoparticles is a central issue in the synthesis of interfacial nanostructures. The size dispersion of growing ensembles is used to characterize the morphology of interfacial structures that are formed by the irreversible deposition of particles or molecules from a bulk solution phase. Brownian Dynamics (BD) simulations have shown considerable potential in providing valuable guidelines for the design and optimization of several aggregation and deposition processes of practical interest.[1−5] The geometric arrangement and distribution of nucleation sites on the surface have been shown to influence the development of size dispersion during the deposition process. For instance, in the case of noninteracting metal ions that nucleate instantaneously and deposit irreversibly, previous studies[4,6] have shown that particle size dispersion of metal nano-ensembles on electrode surface from solution develops when active (nucleation) sites are randomly positioned on the electrode surface. Fransaer and Penner[4] performed BD simulations of diffusion-controlled growth of metal nanoparticles on planar surfaces and found that particles become more size-similar with increasing deposition time provided that active sites are regularly arranged. Therefore, size uniformity can be accomplished by distributing the active sites regularly on the electrode surface.

However, in several systems of practical interest, the distribution of active sites is random.[7] For example, consider the electrocoating of commercial carbon fibers derived from polyacrylonitrile (PAN), where the fiber itself is used as one of the electrodes.[8,9] Such surface treatments have the potential to improve interfacial adhesion when the fiber is used to reinforce polymeric composites and to impart desired mechanical or electrical properties to the fiber. The surface chemistry of the carbon fiber is complex, and the distribution of active sites is random.[10−12] Under such conditions, size dispersion will develop very quickly with increasing deposition time if the monomers nucleate instantaneously and the process is controlled by the diffusion of monomers from the bulk to the surface. Therefore, to obtain uniform coatings, it is important to seek strategies to control the particle size dispersion for such systems.

One of the techniques to reduce size dispersion is to "slow-down" the rate of growth, as demonstrated experimentally in the potentiostatic double-pulse electrodeposition of silver ions.[13−15] In these experiments, a short initial pulse at a high overpotential is used to initiate the formation of the nuclei, and a longer second pulse at lower overpotential is used to control the growth of the nuclei. Corresponding to the double pulse experiments, Penner[5] demonstrated the benefits of slow growth by performing BD simulations for electrodeposition of metal ions on electrode surfaces. In his simulation, Penner[5] considered an ensemble of nuclei initially grown in the diffusion-controlled regime. He further considered a Nernst layer on the electrode surface, so that changing the overpotential could vary the concentration of ions on the electrode surface, and smaller overpotentials lead to slower growth, thereby reducing size dispersion.

* Corresponding author. Phone: +01-314-935-4988. Fax: +01-314-935-7211. E-mail: suresh@wuche.wustl.edu.

10.1021/jp030164c CCC: $25.00
Published on Web 08/28/2003

In this paper, we present a generic framework to incorporate a finite reaction rate between the free particle and the nucleation site, and we also present the results of 3-dimensional BD simulations for the influence of surface reaction rate on the development of size dispersion of interfacial structures that form by instantaneous nucleation and grow on substrates with randomly distributed nucleation sites. The balance of the surface reaction rate to the bulk diffusion rate is incorporated into the BD simulations by using a reaction probability that approaches unity in the case of diffusion-limited growth.[16] For surface-bound electropolymerization, it is anticipated that the surface reaction rate, and hence the reaction probability, can be reduced by decreasing the current density or by changing the electrolyte properties.[8,9,17] This paper is organized as follows: In section 2 we explain and validate the simulation methodology. Section 3 presents the results and discussions. Conclusions are presented in Section 4.

2. Simulation Methodology

In the BD simultaions, we keep track of the coordinates of a set of spherical particles in three dimensions for a dilute system based on the numerical solution of the Langevin equation[18] that represents the force balance for each particle i with mass m in the solution:

$$\mathbf{F}_{\text{total}} = m\frac{\mathrm{d}^2}{\mathrm{d}t^2}\mathbf{r}_i = \sum_j \mathbf{I}_{ij}(r_{ij}) + \mathbf{R}_i + \mathbf{H}_i + \mathbf{F}_{\text{E}} \qquad (1)$$

where $\mathbf{I}$ is the force modeling the interaction between particles, $\mathbf{R}$ is the Brownian force modeling diffusion, $\mathbf{H}$ is the force modeling Stokes viscous drag, and $\mathbf{F}_{\text{E}}$ denotes other possible external forces acting on the particle (e.g., the force of gravity that may be considered when the difference in density between the particle and the solution is large). For time scales larger than the momentum relaxation time, the particle inertia can be neglected, and the motion of the particle is given by the following form of Langevin's equation[19]

$$\mathbf{r}_i(t+\Delta t) = \mathbf{r}_i(t) + (D\Delta t/kT)\left(\sum_j \mathbf{I}_{ij}(r_{ij}) + F_{\text{E}}\right) + \Delta\mathbf{r}^{\text{G}} \qquad (2)$$

where each component of the position vector of a particle at time $t + \Delta t$, $\mathbf{r}_i(t + \Delta t)$, is updated from the position $\mathbf{r}_i(t)$ by taking into account the deterministic displacements due to interactions and external forces and the Brownian (random) displacement $\Delta\mathbf{r}^{\text{G}}$. The components of $\Delta\mathbf{r}^{\text{G}}$ are chosen from a Gaussian distribution with mean equal to zero and variance given by $\langle(\Delta\mathbf{r}^{\text{G}})^2\rangle = 2D\Delta t$, where $D = kT/(6\pi\mu a)$ is the Stokes−Einstein diffusion coefficient, a is the particle radius, k is Boltzmann's constant, T is the temperature, and μ is the fluid viscosity.

For dilute systems, interparticle interactions can be neglected. In addition if no external forces are present, the motion of the particles is due to stochastic displacements and the system asymptotically obeys Einstein's law[1]

$$\mathbf{r}_i(t+\Delta t) = \mathbf{r}_i(t) + \mathbf{g}_{\text{q}}(2D\Delta t)^{0.5} \qquad (3)$$

where $\mathbf{g}_{\text{q}}$ is a vector of Gaussian distributed random numbers with zero mean and variance of unity. We define dimensionless space and time variables as

$$\bar{\mathbf{r}}_i = \frac{\mathbf{r}_i}{a},\ \bar{t} = \frac{D}{a^2}t \qquad (4)$$

TABLE 1: Characteristic Parameters for the Simulation

parameter	value
radius of particle, a (m)	2×10^{-10}
diffusivity of particle, D (m^2/s)	1.2×10^{-9}
no. of particles, N_{tot}	1.515×10^{5}
height of simulation box, L (m)	2.516×10^{-6}
length (and width) of simulation box, S (m)	3.162×10^{-7}
time step, Δt (s)	6×10^{-11}

Then, eq 3 is simplified as

$$\bar{\mathbf{r}}_i(\bar{t} + \Delta\bar{t}) = \bar{\mathbf{r}}_i(\bar{t}) + \mathbf{g}_{\text{q}}(2\Delta\bar{t})^{0.5} \qquad (5)$$

The initial condition in the simulation corresponds to an isothermal, monodispersed, homogeneous system with particle concentration equal to that in the bulk solution. Spherical particles are uniformly distributed within the 3-dimensional rectangular simulation box so that the concentration equals the bulk concentration of 1×10^{-3} M. At the beginning of the simulation, active sites are randomly distributed on the deposition surface, and the number of these active sites is kept constant during the course of the simulation, thereby simulating instantaneous nucleation. We primarily focus on active site density ρ_{n} of 1.44×10^{11} cm^{-2}, although a limited number of simulations were performed for lower values of ρ_{n} to ensure that the results are qualitatively unaffected by the value of ρ_{n}. The nucleation densities used in the simulations are comparable to those reported in earlier studies.[4,5] The active sites are modeled as hemispherical particles having the same radius as the free particles. Sites on the bottom surface of the simulation box except the active ones are inert. A schematic of the simulation cell is shown in Figure 1. The height of the simulation box, L, is calculated based on the total simulation time, t_{f}. Specifically the box height, $L > (2Dt_{\text{f}})^{0.5}$, is kept large enough so that the diffusion front never reaches the top of the simulation box.[20] This ensures that the concenteration at the top of the simulation box remains nearly constant and equal to the bulk concentration. The particles considered in this study are silver ions,[4] and the characterstic simulation parameters are presented in Table 1.

In the simulation, the motions of the free particles in the bulk solution, considered as noninteracting Brownian entities subject to viscous drag, are simulated according to the Einstein's law (eq 5). Periodic boundary conditions are employed in both X and Y directions. Particles are not allowed to escape from the top of the simulation box and the deposition surface, representing the condition that there is no flux in the bulk and across the deposition surface, respectively. If the particle exits the simulation box through the top boundary or the deposition surface, its location is maintained at the particular position at which the particle exits the top of the box (i.e. $z = L$) or deposition surface (i.e. $z = 0$), respectively. This technique is similar to the one used by Nagy et al.[20] The boundary condition is derived from a balance between diffusion and reaction at the surface of a nucleation site. In this study we consider an irreversible first-order surface reaction with lumped surface kinetic rate k_{e}, i.e, in dimensional form

$$k_{\text{e}}C_{r=R} = D\frac{\partial C}{\partial r}\Big|_{r=R} \qquad (6)$$

where C is the particle concentration and r is the radial distance measured from the center of the nucleus of radius R. Such a mixed (Robin-type) boundary condition on the surface has been used to model electrochemical growth of metal nanoparticles. In these processes, ions of the depositing metal diffuse to the

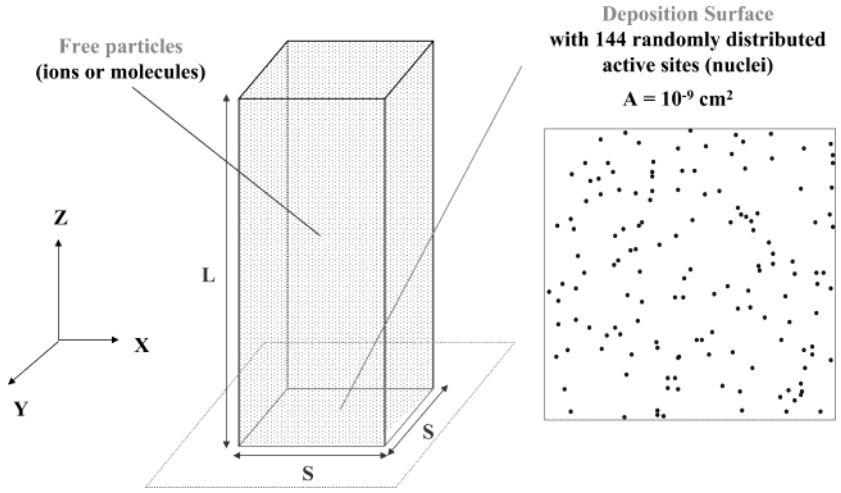

Figure 1. The schematic of the 3-dimensional simulation box and the deposition surface (not drawn to scale).

nuclei, and are discharged and deposited at the surface of the nuclei.[21,22] Equation 6 can be expressed in dimensionless form, as eq 7, using the scales introduced in eq 4 and $\bar{C} \equiv C/C_b$, where C_b is the bulk concentration[8,16,23] as

$$(1 - P_s)\frac{\partial \bar{C}}{\partial \bar{r}}|_{\bar{r}=\bar{R}} - P_s \bar{C}|_{\bar{r}=\bar{R}} = 0 \qquad (7)$$

where the reaction probability, P_s, represents the relative ratio of the kinetic rate of attachment to the rate of diffusion from bulk to the surface, i.e.,

$$P_s = \frac{\mathrm{Da}}{1 + \mathrm{Da}} \qquad (8)$$

where Da is the Damkohler number defined as $\mathrm{Da} \equiv k_e a/D$. P_s is interpreted as the probability of reaction to take place once a free particle reaches a nucleation site. The limit $P_s \rightarrow 1$ denotes growth limited by the diffusion of the particles from the bulk to the surface, and $P_s \ll 1$ indicates that the whole process is controlled by the reaction at the surface of the nucleating site. In the course of the simulation, when the free particles come into contact with any of the active sites on the surface they will attach on it with a finite reaction probability P_s.[16] Once the particle has reacted with the nucleus, the radius of the hemispherical nucleus is increased in such a way that the volume of the hemispherical nucleus is increased by an amount equal to the volume of the free particle. This is done so that the growth of the nuclei is consistent with the Volmer−Weber growth mechanism as observed experimentally for the deposition of silver ions on low surface free energy surfaces.[24] A similar approach has been used in previous simulations of growth of metal nanoparticles on electrode surfaces.[4,5,20] The reacted particle is then removed from the simulation and the total number of reacted particles is incremented.[20]

One of the advantages of this generic approach is that for realistic systems (e.g., carbon fibers) with unknown or poorly characterized surface−particle interactions, the value of P_s can be determined from experiments. By comparing the average flux and/or concentration profiles obtained experimentally with classical convection−diffusion models with reactive boundary conditions, the P_s can be determined. This experimental data might include image analysis of the TEM/SEM or gravimetric measurements for the longer time deposition experiments. As done in previous studies,[4,6] the reliability of our simulation algorithm in a rectangular simulation box for modeling the instantaneous nucleation followed by the growth of the nuclei

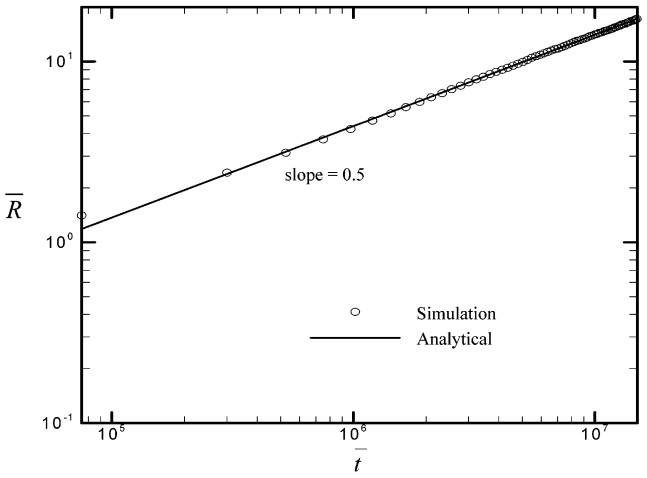

Figure 2. Growth of a single nucleus as a function of time on the log scale averaged over four replicate simulations. Error bars are comparable to symbol size.

is verified for the case of diffusion controlled growth ($P_s = 1$) of a single isolated nucleus growing on a planar surface. The radius of a growing nucleus in the dimensionless form (using eq 4) is given by[25]

$$\bar{R}(\bar{t}) = \left[\frac{2C_b M \bar{t}}{\rho}\right]^{0.5} \qquad (9)$$

where $\bar{R}(\bar{t})$ is the dimensionless radius of the nucleus, M is the molecular weight of particles, and ρ is the density of the particles. Figure 2 shows the evolution of the radius of a single nucleus growing at the center of the simulation box as a function of time. The agreement between BD simulations and the analytical expression is very good for the entire 0.5-ms period of the simulation.

3. Results and Discussion

The simulation results presented in this section required approximately between 5 and 7 days on an Intel Pentium P4 2.5-GHz workstation, with the lower nucleation density and lower reaction probability simulations requiring more computational time. The BD simulation results presented here correspond to an ensemble average of four realizations obtained by using different initial conditions of the active sites on the deposition surface and the different initial configurations of the free particles. The results in this section have been made

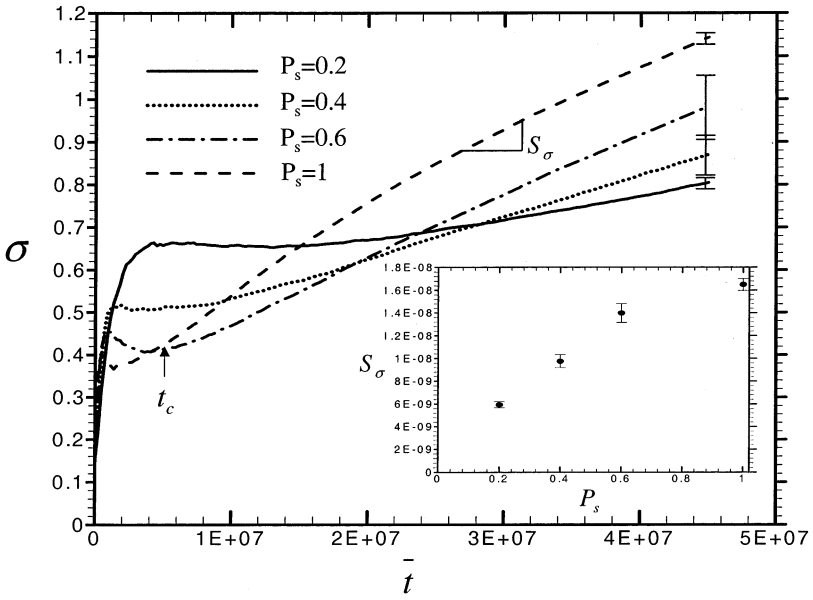

Figure 3. The standard deviation of the particle radius, $\sigma(t)$, as a function of time for different reaction probabilities for $\rho_n = 1.44 \times 10^{11}$ cm^{-2}. Error bars represent 1σ for $\sigma(t)$ obtained from four replicate simulations at each P_s. Inset shows the slope, S_σ, of standard deviation versus time plots at different values of P_s.

dimensionless according to eq 4, and the dimensional final time in the simulations is 1.5 ms. Error bars shown in the results indicate one standard deviation of the result that was calculated for the four simulations performed with different seeds for the random number generator.

To investigate the temporal evolution of the particle size dispersity, the standard deviation of the radii of all the growing ensembles on the deposition surface, $\sigma(t)$, is used as a quantitative measure. Figure 3 shows the temporal evolution of the particle size dispersion for four different values of reaction probability, ranging from 0.2 to 1.0. When the reaction probability P_s is equal to 1, the free particles aggregate instantaneously to the growing nuclei on the active sites, and the particle growth is therefore diffusion limited. When the reaction probability decreases, the particle growth becomes slower, and consequently the aggregation gradually becomes reaction controlled. The evolution of the standard deviation with time has similar qualitative trends irrespective of the value of P_s. The size dispersion initially increases rapidly for short times. This is followed by a time period until $t = t_c$ in Figure 3 during which the standard deviation decreases or remains practically unchanged. For $t > t_c$, $\sigma(t)$ increases with increasing time. However, differences exist among the evolution of σ for different P_s values. Specifically, the long-time evolution of the standard deviation changes from a slow increase for $P_s = 0.2$ to a rapid increase for $P_s = 1$. As shown in the inset in Figure 3, the slope of the linear best fit of the σ vs t curve at long times, S_σ, increases with reaction probability P_s. We further investigated whether the density of active sites, ρ_n, could influence the behavior of the σ vs t curves by performing simulations for $\rho_n = 3.6 \times 10^{10}$ cm^{-2}. These results are reported in Figure 4. As can be seen from Figure 4, the influence of P_s on σ is qualitatively independent of ρ_n. Comparison of Figures 3 and 4 shows that for a given P_s, σ is lower for the surface with lower ρ_n. This implies that the size monodispersity of particles can be improved by decreasing the nucleation density on the surface. This result is consistent with experiments in which the relative size monodispersity of particles was found to improve by lowering ρ_n via decreasing the overpotential of the growth pulse.[14]

The transients in particle standard deviation for $t < t_c$ are similar to those obtained in a previous BD study of diffusion-

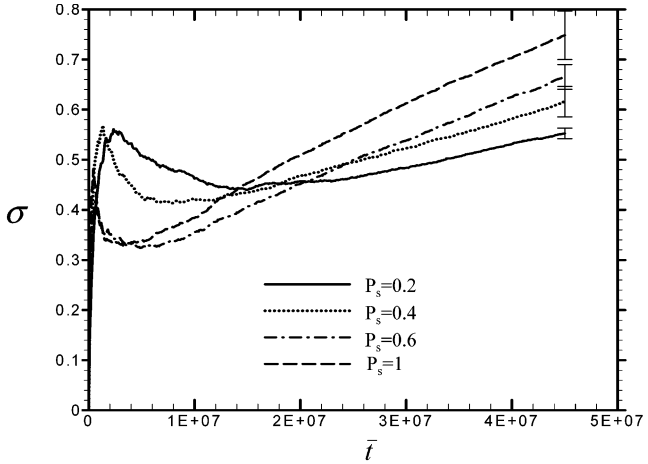

Figure 4. The standard deviation of the particle radius, $\sigma(t)$, as a function of time for different reaction probabilities for $\rho_n = 3.6 \times 10^{10}$ cm^{-2}. Error bars represent 1σ for $\sigma(t)$ obtained from four replicate simulations at each P_s.

controlled growth of metal nanoparticles, and can be explained by the stochastic nature of the deposition process.[4] For $t > t_c$, the diffusion zones surrounding the growing nucleus overlap, and the flux of the particles is spatially uniform on the deposition surface. It can be shown that the time at which σ begins to increase in the simulations, t_c, is correlated to the time, $t_{overlap}$, at which the diffusion zones of neighboring nuclei overlap. The concentration profile around a spherical nucleus can be obtained by solving the diffusion equation in spherical coordinates. In the dimensionless form

$$\frac{\partial \bar{C}}{\partial \bar{t}} = \frac{1}{\bar{r}^2}\frac{\partial}{\partial \bar{r}}\left(\bar{r}^2 \frac{\partial \bar{C}}{\partial \bar{r}}\right) \tag{10}$$

$$\bar{C}(\bar{r},0) = \bar{C}(\infty,\bar{t}) = 1 \tag{10a}$$

$$(1 - P_s)\frac{\partial \bar{C}}{\partial \bar{r}}|_{\bar{r}=\bar{R}} - P_s \bar{C}|_{\bar{r}=\bar{R}} = 0 \tag{10b}$$

The concentration of particles around the growing nucleus can be obtained by the solution of eqs 10−10b as[26]

$$\bar{C}(\bar{r},\bar{t}) = 1 - \left(\frac{\bar{R}-\bar{\gamma}}{\bar{r}}\right)\left(\mathrm{erfc}\left(\frac{\bar{r}-\bar{R}}{2\sqrt{\bar{t}}}\right) + \exp\left(\frac{\bar{t}}{\bar{\gamma}^2} + \frac{\bar{r}-\bar{R}}{\bar{\gamma}}\right)\mathrm{erfc}\left(\frac{\sqrt{\bar{t}}}{\bar{\gamma}} + \frac{\bar{r}-\bar{R}}{2\sqrt{\bar{t}}}\right)\right) \quad (11)$$

where

$$\bar{\gamma} = \frac{1}{\frac{P_s}{1-P_s} + \frac{1}{\bar{R}}}$$

and, erfc(x) is the complementary error function defined as

$$\mathrm{erfc}(x) = 1 - \frac{2}{\sqrt{\pi}}\int_0^x \exp(-y^2)\,dy$$

The growth of the radius of a single nucleus can be obtained by considering a mass balance for the nucleus[6,22]

$$\frac{\partial \bar{C}}{\partial \bar{r}}\Big|_{\bar{r}=\bar{R}} = \frac{MC_b}{\rho}\frac{d\bar{R}}{d\bar{t}} \quad (12)$$

where $\bar{R}$ is the dimensionless radius of the nucleus. The radius as a function of time is given by[22]

$$\bar{R}(\bar{t}) = \left[\left(\frac{1-P_s}{P_s}\right)^2 + \left(\frac{2C_bM\bar{t}}{\rho}\right)\right]^{0.5} - \frac{1-P_s}{P_s} \quad (13)$$

Note that for the case of diffusion controlled growth ($P_s = 1$), eq 13 reduces to eq 9.

Using eqs 11 and 13, the concentration profile around a spherical nucleus can be completely determined. The dimensionless diffusion layer radius, $\bar{R}_d$, is taken to be that radius at which the dimensionless concentration of the diffusion layer equals 0.9.[7] $\bar{R}_d$ can then be obtained by solving for $\bar{r}$ as a function of $\bar{t}$ by setting $\bar{C} = 0.9$ in eq 11. Figure 5 shows the evolution of the radius of the diffusion layer, $\bar{R}_d$, for the case of $P_s = 1$ and 0.2. In the case of diffusion-controlled growth ($P_s = 1$), the radius of the diffusion layer is found to be proportional to square root of time, consistent with earlier reported trends.[7] The time $t_{overlap}$ is the time at which the radius of the diffusion zone is half the average nearest neighbor distance. Figure 6a shows t_c from BD simulations, and $t_{overlap}$ predicted by the continuum diffusion equation, for the four different values of P_s and different values of ρ_n. A strong correlation is seen between the two times, thereby indicating that the diffusion layer is approximately planar across the entire deposition surface when the standard deviation in the simulation starts increasing. As expected, t_c and $t_{overlap}$ are higher for the lower value of ρ_n. This can be explained by the larger average nearest neighbor distance for the lower ρ_n, necessitating larger time intervals for the diffusion layers to overlap (see Figure 5). Further, as P_s decreases, t_c and $t_{overlap}$ increase. An order of magnitude difference can be seen between the values of t_c and $t_{overlap}$ obtained for $P_s = 0.2$ and 1. This can be explained by the smaller diffusion zones surrounding a particle growing at lower P_s (Figure 5).

It should be noted that an exact quantitative agreement between t_c and $t_{overlap}$ does not exist. This can be attributed to the simplification in the mathematical analysis that considers the concentration profiles around a growing nucleus to be that of an isolated nucleus and an average nearest neighbor distance rather than a distribution of nearest neighbors distances.

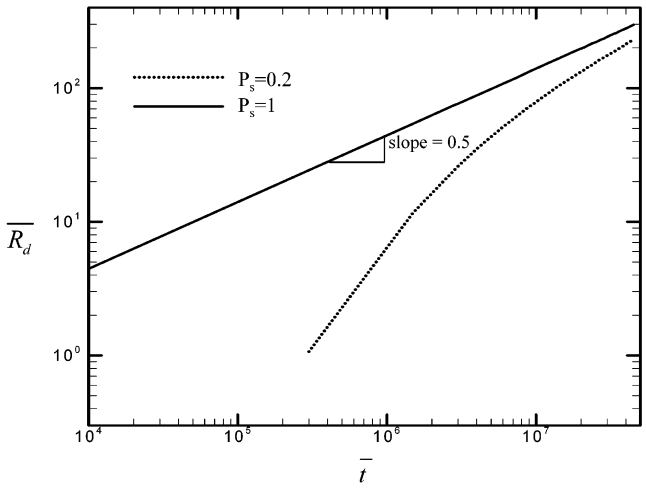

Figure 5. The radius of the diffusion layer, $\bar{R}_d$, as a function of time for $P_s = 1.0$ and 0.2 on log scale.

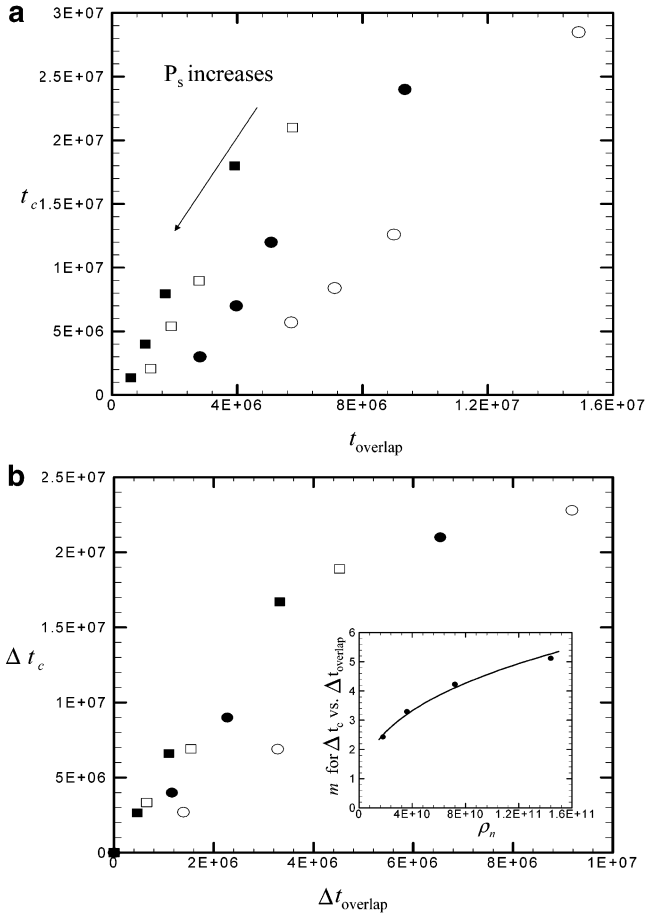

Figure 6. (a) The time for diffusion layer overlap from the BD simulations, t_c, versus time for diffusion layer overlap predicted by continuum equations for isolated nucleus, $t_{overlap}$, at four different values of P_s for $\rho_n = 1.44 \times 10^{11}$ (■), 7.2×10^{10} (□), 3.6×10^{10} (●), and 1.8×10^{10} cm^{-2} (○). (b) Plot of Δt_c versus $\Delta t_{overlap}$ at four different values of P_s for $\rho_n = 1.44 \times 10^{11}$ (■), 7.2×10^{10} (□), 3.6×10^{10} (●), and 1.8×10^{10} cm^{-2} (○). The inset shows the slope of linear best fit of Δt_c versus $\Delta t_{overlap}$ as a function of ρ_n.

However this analysis can be used to estimate t_c for given ρ_n and P_s values. Toward this end, we define two new variables, $\Delta t_c \equiv t_c|_{P_s} - t_c|_{P_s=1}$ and $\Delta t_{overlap} \equiv t_{overlap}|_{P_s} - t_{overlap}|_{P_s=1}$. As shown in Figure 6b, the relationship between Δt_c and $\Delta t_{overlap}$ is linear for all the values of ρ_n considered in this study, i.e., $\Delta t_c = m\Delta t_{overlap}$, where m is a function of ρ_n. The dependence

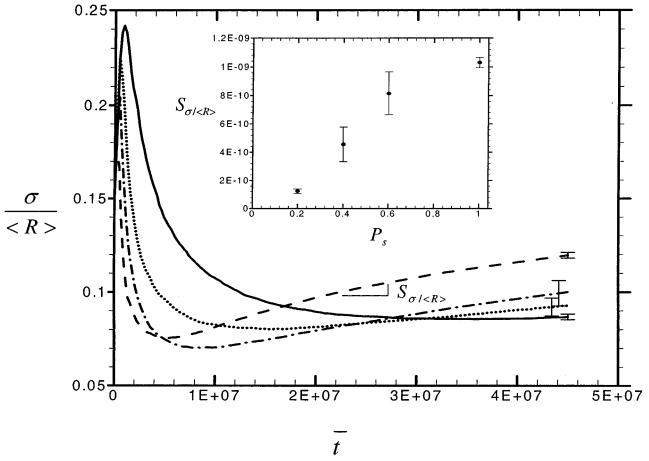

Figure 7. The relative standard deviation of the particle radius, $\sigma/\langle R\rangle$, as a function of time for different reaction probabilities for $\rho_n = 1.44 \times 10^{11}$ cm^{-2}. Error bars represent 1σ of $\sigma/\langle R\rangle$ for four different replicates of the simulations. The legend is the same as for Figure 3. The inset shows the slope $S_{\sigma/\langle R\rangle}$ of standard deviation versus time plots for different values of P_s.

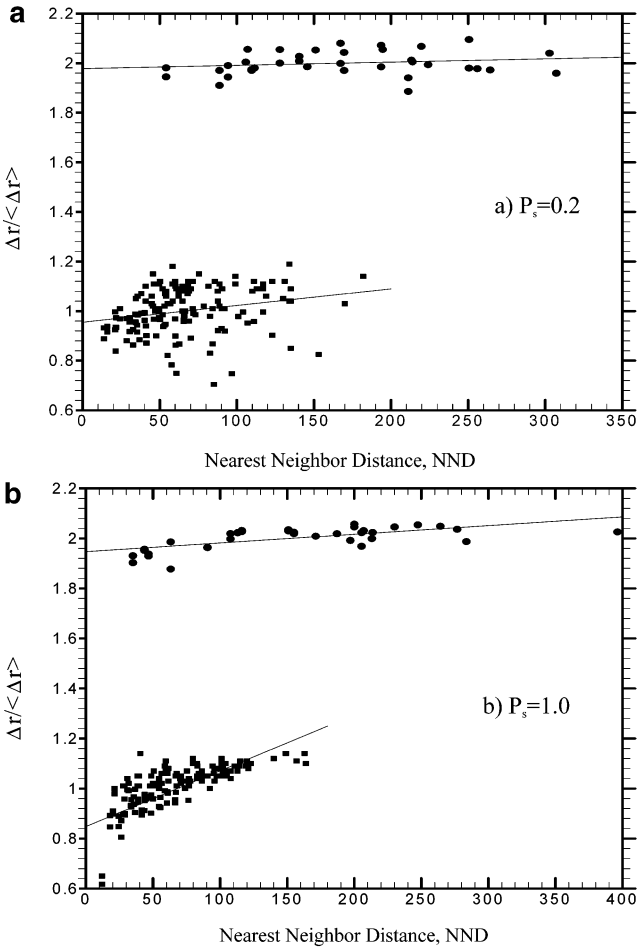

Figure 8. Particle growth, $\Delta r/\langle\Delta r\rangle$, versus the nearest neighbor distance for one simulation performed at (a) $P_s = 0.2$ and (b) 1 for $\rho_n = 1.44 \times 10^{11}$ (■) and 3.6×10^{10} cm^{-2} (●). Results for $\rho_n = 3.6 \times 10^{10}$ cm^{-2} have been increased by one unit for clarity. Lines represent the best fit obtained by least-squares analysis of the data.

of m on ρ_n is shown in the inset of Figure 6b. It is found that the slope of this best-fit line follows a power law relationship given by $m \propto \rho_n^{0.36}$.

The relative size dispersity (RSD) of the growing nanoparticles (characterized by the ratio of the standard deviation to the mean radius, $\sigma/\langle R\rangle$) is shown in Figure 7. At long deposition times, the RSD remains nearly constant at low values of P_s and increases with time for larger P_s. Moreover, as shown in the inset in Figure 7, the slope of the linear best fit of $\sigma/\langle R\rangle$ vs time curve at long times, $S_{\sigma/\langle R\rangle}$, increases rapidly as the P_s increases. This observation leads to the conclusion that a strategy to improve the size uniformity of particles growing on a random distribution of nucleating sites on a deposition surface would be to reduce the reaction probability P_s and thereby slow the growth of the nanoensembles.

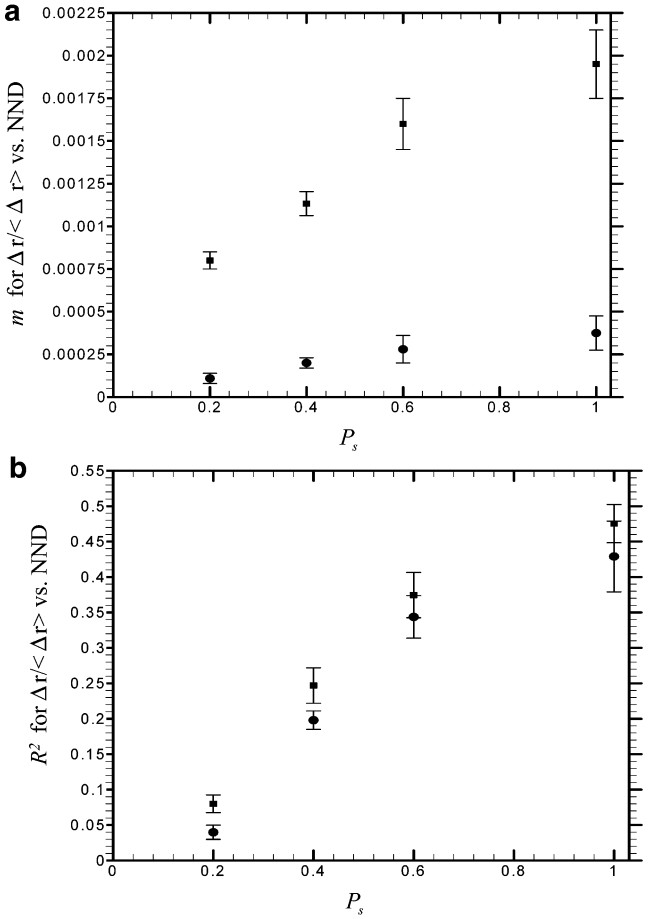

Figure 9. Plot of (a) the slope, m, and (b) regression coefficient, R^2, of the best-fit line in Figure 8 vs P_s for $\rho_n = 1.44 \times 10^{11}$ (■) and 3.6×10^{10} cm^{-2} (●). Error bars in the plot represent 1σ from four different replicates at each value of P_s.

These results for σ and RSD of growing nanoparticles can be explained by the dependence of the growth of the particles on a surface to the distance of the particle to its nearest neighbor, NND from here onward. A previous study of diffusion-limited growth of nanoparticle ensembles randomly distributed on deposition surface showed an increase in the growth of nearest neighbors as the proximity between the particles increased.[4] This phenomenon of retardation in the growth of densely nucleated regions has been referred to as interparticle diffusional coupling.[4,5] In our simulations we investigate the effect of P_s on interparticle diffusional coupling. Toward this end, we compute the increase in the radii of each active site, $\Delta r \equiv r(t) - a$, normalized with respect to its ensemble average value $\langle\Delta r\rangle$ for different times. Panels a and b in Figure 8 show results from a single simulation of $\Delta r/\langle\Delta r\rangle$, as a function of NND obtained for the two different ρ_n values for $P_s = 0.2$ and 1, respectively. It can be seen from these figures that there exists a stronger linear correlation between the growth of particles and the NND

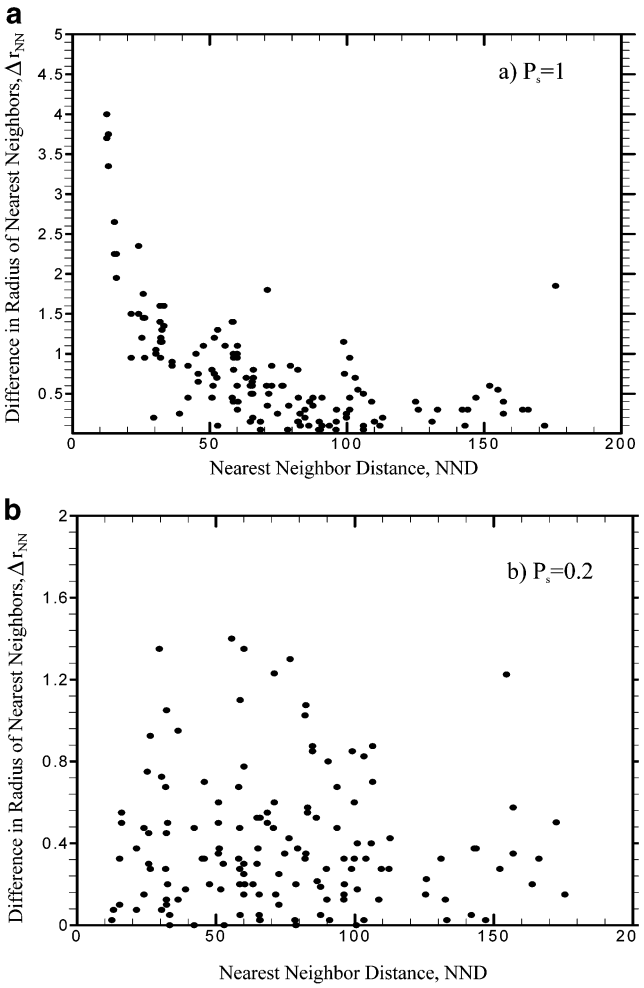

Figure 10. Plot of the difference in radii of nearest neighbors, Δr_{NN}, as a function of nearest neighbor distance from a single simulation for (a) $P_s = 1.0$ and (b) 0.2 and $\rho_n = 1.44 \times 10^{11}$ cm^{-2}.

for $P_s = 1$ as compared to that observed for $P_s = 0.2$. This correlation between the particle growth and NND is seen in the simulations with lower ρ_n as well (Figure 8a,b). The linear correlation is stronger for the higher value of ρ_n, consistent with the increase in interparticle diffusional coupling with increasing ρ_n. Simulations at other values of P_s support the conclusion that lower values of P_s lead to a reduced correlation between particle radii and NND. This is quantitatively shown in Figure 9a,b, where the slope, m, and regression coefficient, R^2, of the linear best fit of the $\Delta r/\langle \Delta r \rangle$ vs NND data are plotted as a function of P_s for the two values of ρ_n. Both m and R^2 increase with increasing P_s, similar to the increase in S_σ and $S_{\sigma/\langle R \rangle}$ with increasing P_s. Further, m and R^2 are lower for the lower nucleation density at all P_s. This leads to the conclusion that lower reaction probabilities and lower nucleation densities reduce the interparticle diffusional coupling between neighboring particles, leading to reduced RSD.

In addition to the good correlation of the $\Delta r/\langle \Delta r \rangle$ with NND, a correlation of the difference in radii of the nearest neighbors and NND is observed for diffusion-controlled growth ($P_s = 1$). As shown in Figure 10a, as the NND increases, the difference in the radii of the nearest neighbor decreases. This result can be explained by disparity in the particle flux between the nearest neighbors as the distance between them decreases.[4] This implies that when NND is small, the larger particle receives a larger fraction of the total flux, and hence larger particles grow at a faster rate. This causes further enhancement in the size dispersion. However, no significant correlation is seen between the difference in the radii of nearest neighbors and the NND for $P_s = 0.2$, as shown in Figure 10b. In this case the difference in the distribution of fluxes between nearest neighbors is reduced due to the fact that when a moving particle strikes the nucleation site, it does not necessarily nucleate instantaneously as in the case of $P_s = 1$. Hence a free particle samples a larger number of nucleating sites before it sticks to one of them. Thus for lower P_s, the interface is growing more uniformly, leading to a reduction in RSD.

4. Conclusions

In this paper, we have developed a Brownian Dynamics Simulation framework to investigate the effect of surface kinetics on the size dispersion of randomly distributed nuclei growing under instantaneous nucleation. A reaction probability P_s was introduced into the simulations, to account for the different modes of growth, ranging from diffusion controlled at $P_s = 1$ to surface reaction controlled for $P_s \ll 1$. The reaction probability can be explicitly evaluated as a function of the Damkholer number that represents the ratio of the surface reaction rate to the bulk diffusion rate of mass transfer. When the active sites are randomly positioned on the electrode surface as in the case of carbon fibers, the simulations show that size dispersion will develop after the diffusion layers surrounding the growing nuclei overlap. However, the time required for this overlap to occur can be manipulated (by orders of magnitude) by changing the reaction probability. Specifically a strategy for improving the size uniformity, characterized by the relative size dispersion, is to reduce the reaction probability, and therefore slow the surface reactions. The 3-dimensional Brownian Dynamics Simulation technique presented here can be used to study a wide variety of other problems, including colloidal deposition, progressive nucleation processes, and biological aggregate formation. These BD simulation results can potentially be used as qualitative guidelines for synthesizing dimensionally uniform electropolymerized coatings on carbon fiber surface with desired micromorphology.

Acknowledgment. The authors gratefully acknowledge financial support from the Boeing Company.

References and Notes

(1) Bos, M. T. A.; van Opheusden, J. H. J. *Phys. Rev. E* **1996**, *53*, 5044.
(2) Oberholzer, M. R.; Wagner, N. J.; Lenhoff, A. M. *J. Chem. Phys.* **1997**, *107*, 9157.
(3) Gray, J. J.; Bonnecaze, R. T. *J. Chem. Phys.* **2001**, *114*, 1366.
(4) Fransaer, J. L.; Penner, R. M. *J. Phys. Chem. B* **1999**, *103*, 7643.
(5) Penner, R. M. *J. Phys. Chem. B* **2001**, *105*, 8672.
(6) Cao, Y.; Searson, P. C.; West, A. C. *J. Electrochem. Soc.* **2001**, *148*, C376.
(7) Serruya, A.; Mostany, J.; Scharifker, B. R. *J. Chem. Soc., Faraday Trans.* **1993**, *89* (2), 255.
(8) Lin, B.; Sureshkumar, R.; Kardos, J. L. *Chem. Eng. Sci.* **2001**, *56*, 6563.
(9) Lin, B.; Sureshkumar, R.; Kardos, J. L *Chem. Eng. Sci.* **2003**, *58*, 2445.
(10) Hughes, J. D. H. *Compos. Sci. Technol.* **1991**, *41*, 13.
(11) Donnet, J. B.; Qin, R. Y. *Carbon* **1993**, *31* (1), 7.
(12) Nakao, F.; Takenaka, Y.; Asai, H. *Composites* **1992**, *23*, 365.
(13) Liu, H.; Penner, R. M. *J. Phys. Chem. B* **2000**, *104*, 9131.
(14) Liu, H.; Favier, F.; Ng, K.; Zach, M. P.; Penner, R. M *Electrochim. Acta* **2001**, *47*, 671.
(15) Sandman, G.; Dietz, H.; Plieth, W. *J. Electroanal. Chem.* **2000**, *491*, 78.
(16) Lin, B.; Sureshkumar, R.; Kardos, J. L. *Ind. Eng. Chem. Res.* **2002**, *41*, 1189.

(17) Lin, B. D. Sc. Dissertation, Washington University, St. Louis, 2002.
(18) Russel, W. B.; Saville, D. A.; Schowalter, W. R. *Colloidal Dispersions*; Cambridge University Press Inc.: New York, 1989.
(19) Ermak, D. L. *J. Chem. Phys.* **1975**, *62* (10), 4189.
(20) Nagy, G.; Sugimoto, Y.; Denuault, G. *J. Electroanal. Chem.* **1997**, *433*, 167.
(21) Cao, Y.; West, A. C. *J. Electrochem. Soc.* **2002**, *149* (4), C223.
(22) Fletcher, S. *J. Chem. Soc., Faraday Trans. 1* **1983**, *79*, 467.
(23) Nagatani, T. *Phys. Rev. A* **1989**, *40*, 7286.
(24) Zoval, J. V.; Stiger, R. M.; Biernacki, P.; Penner, R. M. *J. Phys. Chem.* **1996**, *100*, 837.
(25) Scharifker, B.; Hills, G. *J. Electroanal. Chem.* **1981**, *130*, 81.
(26) Collins, F. C.; Kimball, G. E. *J. Colloid Interface Sci.* **1949**, *4*, 425.